Moderately nonlinear diffuse-charge dynamics under an ac voltage

Robert F. Stout and Aditya S. Khair

Phys. Rev. E **92**, 032305 — Published 9 September 2015

DOI: 10.1103/PhysRevE.92.032305

Moderately nonlinear diffuse charge dynamics under an AC voltage

Robert F. Stout and Aditya S. Khair
Department of Chemical Engineering, Carnegie Mellon University, Pittsburgh, PA 15213 USA
(Dated: August 21, 2015)

The response of a symmetric binary electrolyte between two parallel, blocking electrodes to a moderate amplitude AC voltage is quantified. The diffuse charge dynamics are modeled via the Poisson-Nernst-Planck equations for a dilute solution of point-like ions. The solution to these equations is expressed as a Fourier series with a voltage perturbation expansion for arbitrary Debye layer thickness and AC frequency. Here, the perturbation expansion in voltage proceeds in powers of $V_o/(k_BT/e)$ where V_o is the amplitude of the driving voltage and k_BT/e is the thermal voltage with k_B as Boltzmann's constant, T as the temperature, and e as the fundamental charge. We show that the response of the electrolyte remains essentially linear in voltage amplitude at frequencies greater than the RC frequency of Debye layer charging, $D/\lambda_D L$, where D is the ion diffusivity, λ_D is the Debye layer thickness, and L is half the cell width. In contrast, nonlinear response is predicted at frequencies below the RC frequency. We find that the ion densities exhibit symmetric deviations from the (uniform) equilibrium density at even orders of the voltage amplitude. This leads to the voltage dependence of the current in the external circuit arising from the odd orders of voltage. For instance, the first nonlinear contribution to the current is $O(V_o^3)$ which contains the expected third harmonic but also a component oscillating at the applied frequency. We use this to compute a generalized impedance for moderate voltages, the first nonlinear contribution to which is quadratic in V_o. This contribution predicts a decrease in the imaginary part of the impedance at low frequency, which is due to the increase in Debye layer capacitance with increasing V_o. In contrast, the real part of the impedance increases at low frequency, due to adsorption of neutral salt from the bulk to the Debye layer.

I. INTRODUCTION

The dynamics of electrolyte solutions exposed to an applied or induced time-dependent electric potential is exploited in desalination and deionization[1–4], microfluidics[5–8], and the manipulation of colloidal particles[9–12] and biological cells[13, 14], among other applications. The abundant historical work indicates diffuse charge dynamics of electrolytes is well understood for applied potentials below the thermal voltage, k_BT/e, where k_B is the Boltzmann constant, T is temperature, and e is the fundamental charge (see [15] and references therein). For reference, $k_BT/e \approx 25$ mV at $T = 298$ K. For instance, the majority of work in electrokinetics over the last century has considered fluid flow or particle motion driven by weak applied potentials, $V < k_BT/e$[16], for which the equilibrium diffuse screening layer, or "Debye layer," around a charged surface or particle is only slightly perturbed. In contrast, modern applications such as AC, induced-charge, or second-kind, electro-osmotic pumps [17–21], and electrochemical supercapacitors[22, 23] use time-dependent potentials on the order of a few volts, well above the thermal voltage. The relative scarcity of theoretical treatment for such larger voltages creates a need to study diffuse charge dynamics in this regime, where the Debye layer can be driven strongly out of equilibrium.

Perhaps the simplest model system for which nonlinear diffuse charge dynamics can be analyzed is a dielectric solvent containing a symmetric, binary, monovalent electrolyte between two perfectly blocking (non-reactive) electrodes a distance $2L$ apart (figure 1). A voltage is applied across this electrochemical cell and the ions form Debye layers near the electrodes to screen the resulting surface charge. For the purposes of the present paper, we take this voltage to be $V(t) = V_o \cos(\omega t)$, where V_o is the voltage amplitude, ω is the frequency, and t is time. For dilute solutions, the characteristic size of the Debye layer is given by the Debye length, $\lambda_D = \sqrt{\varepsilon k_BT/2e^2n_0}$, where ε is the dielectric permittivity of the solvent and n_0 is the initial (uniform) ion number density.

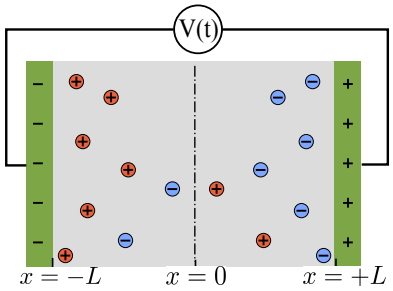

FIG. 1: (Color online) Ions are initially uniformly dispersed in a dielectric liquid between two perfectly blocking electrodes. A voltage $V(t) = V_o \cos(\omega t)$ is applied across the cell and charge transport occurs normal to the electrode surface.

The Poisson-Nernst-Planck (PNP) equations for point-sized, non-interacting ions are conventionally used to model the charge transport in this system. These equations are nonlinear and cannot be solved analytically, in general. For small voltages, $V(t) < k_BT/e$, the equa-

tions can be linearized and analytical solutions can be derived[15]. Solutions to the linearized PNP equations are useful in electrochemical impedance spectroscopy (EIS), which is a technique used to measure electrical properties of a charge carrying system such as capacitance and conductivity[24].

EIS is primarily based on the assumption that an oscillating voltage $V(t) = V_o \cos(\omega t)$ will generate a current, $I(t)$, through an external circuit that is linear in the voltage amplitude, V_o. An impedance is then defined as $Z = V(t)/I(t)$ and will be a function of frequency only. The linearized PNP equations can be used to derive analytical formula for the impedance[24–26]. Expressed as a complex number, the real (in-phase) part of the impedance corresponds to the resistive nature of the electrolyte via its conductivity; the complex (out-of-phase) part corresponds to the capacitive nature of the Debye layers and the dielectric solvent. At large voltages, $V_o > k_BT/e$, the diffuse charge dynamics are no longer linear; hence the current contains harmonic overtones and its amplitude is not linearly proportional to V_o[25–28]. Thus, larges voltages are typically avoided when measuring impedance.

A handful of works have focused on the nonlinear response of electrolytes to AC voltages. Freire *et al.* [26] numerically solved the PNP equations and showed that the electrolyte response becomes increasingly linear as ω increases, regardless of V_o. That is, as ω increases for a fixed V_o, the external current eventually loses harmonic overtones and simply oscillates with the frequency of the driving voltage. Olesen *et al.*[27] examined the long-time periodic response to a voltage oscillating near the RC frequency, $\omega \approx D/\lambda_D L$, where D is the diffusivity of the ions. They solved the PNP equations numerically and also performed asymptotic analysis in the thin-Debye-layer limit $\lambda_D/L \to 0$. They define a "weakly-nonlinear" regime where the electroneutral bulk electrolyte (outside the Debye layers) retains a uniform "neutral salt" concentration (total ion concentration), and the nonlinear response is driven solely by the nonlinear capacitance of the Debye layers. Schnitzer and Yariv[28] derived an asymptotic current-voltage relationship for this regime as $V_o \to \infty$. Olesen *et al.*[27] also analyzed "strongly-nonlinear" response at very large voltages. Here, there is significant ion depletion adjacent to the Debye layers, which leads to "AC capacitive desalination" as a net flux of salt is transferred from the bulk to the Debye layer during an oscillation period. Furthermore, at such large voltages the Debye layers can attain a non-equilibrium structure, characterized by the periodic growth and shrinkage of transient space-charge layers.

In this work, we consider electrolyte dynamics under an AC field with amplitude $V_o \sim 1 - 10 k_BT/e$, at arbitrary Debye layer thickness λ_D/L and across a wide range of frequencies ω. We refer to this as the "moderately nonlinear" regime of diffuse charge dynamics, to distinguish our work from the articles mentioned above. Notably, the thin-Debye-layer limit $\lambda_D/L \ll 1$ is commonly assumed in mathematical analysis of electrolyte dynamics. However, this can be violated in nano-scale electrochemical systems, where the electrode separation $2L$ approaches the Debye length λ_D: e.g., in nanometer wide thin-layer cells used to probe fast electron-transfer kinetics [29]. We use a complex Fourier series to decompose the electrolyte dynamics into its component harmonics and a perturbation expansion in voltage for the Fourier coefficients. A similar approach was recently utilized by Bandopadhyay *et al.*[30]; however, their expansion stopped at $O(V_o^2)$. We proceed to $O(V_o^3)$, which is necessary to predict a nonlinear current response for a symmetric, binary electrolyte. We also derive a first approximation to a voltage dependent impedance that is $O(V_o^2)$.

The paper is organized as follows: in section 2 we present the mathematical model to calculate the moderately nonlinear dynamics. In section 3, we present the results for the ion dynamics and external current. In section 4, we calculate a voltage-dependent "impedance" as the current first becomes nonlinear in V_o. Conclusions are offered in section 5.

II. MATHEMATICAL MODEL

We consider the prototypical situation (figure 1) of two parallel, perfectly blocking electrodes separated by a dielectric solvent containing an ideal solution of monovalent, point-like charge carriers. We assume that the electrodes are spaced sufficiently close such that the charge transport persists perpendicular to the electrode surface. The one dimensional PNP equations are

$$\varepsilon \frac{\partial^2 \phi}{\partial x^2} = -\rho = -e(n_+ - n_-), \tag{1a}$$

$$\frac{\partial n_r}{\partial t} = -\frac{\partial j_r}{\partial x} = D\left[\frac{\partial^2 n_r}{\partial x^2} + r\frac{e}{k_BT}\frac{\partial}{\partial x}\left(n_r \frac{\partial \phi}{\partial x}\right)\right]. \tag{1b}$$

Equation (1a) is Poisson's equation describing the electrostatic potential, ϕ, in response to the ionic charge density, ρ, which undergoes changes in time and space according to the ion flux balance (1b), where n_r is the ion number density of cations ($r = +$) and anions ($r = -$), t is time, x is the position across the cell, and j_r is the ion flux.

We supplement the governing equations with the following boundary conditions:

$$\phi(x = \pm L, t) = \pm V_o \cos(\omega t), \tag{2a}$$

$$j_r(x = \pm L, t) = -D\left[\frac{\partial n_r}{\partial x} + r\frac{e}{k_BT} n_r \frac{\partial \phi}{\partial x}\right]_{\pm L} = 0, \tag{2b}$$

specifying that the electrode surface potential is equal to the applied potential (2a) and no ion flux through the

electrodes (2b). By using these boundary conditions, we seek to find the steady periodic response as opposed to suddenly applying an AC voltage to a previously unaffected system. Note that from (2a), the total applied potential across the cell is $2V_o$.

We non-dimensionalize as follows: position (x) with half the cell width (L), electrostatic potential (ϕ) with thermal voltage (k_BT/e), ion density (n_r) with the uniform ion density (of a single species) prior to the application of a voltage (n_0), time (t) with the RC time for Debye layer charging ($\lambda_D L/D$)[15], and frequency (ω) with the RC frequency. Recall that $\lambda_D = \sqrt{\varepsilon k_B T/2e^2 n_0}$ is the Debye length. The non-dimensional governing equations are then

$$\frac{\partial^2 \phi}{\partial x^2} = -\frac{n_+ - n_-}{2\epsilon^2}, \tag{3a}$$

$$\frac{\partial n_r}{\partial t} = \epsilon \left[\frac{\partial^2 n_r}{\partial x^2} + r \frac{\partial}{\partial x}\left(n_r \frac{\partial \phi}{\partial x} \right) \right], \tag{3b}$$

where $\epsilon = \lambda_D/L$ and all quantities in (3) and onward, unless stated otherwise, are dimensionless. The corresponding non-dimensional boundary conditions are

$$\phi(x = \pm 1, t) = \pm \mathcal{V}_o \cos(\omega t), \tag{4a}$$

$$\left[\frac{\partial n_r}{\partial x} + r n_r \frac{\partial \phi}{\partial x} \right]_{\pm 1} = 0, \tag{4b}$$

where $\mathcal{V}_o = V_o/(k_BT/e)$ is the dimensionless applied voltage amplitude.

For small amplitude voltages, $\mathcal{V}_o < 1$, it is typical to express ϕ and n_r as complex valued functions of ω that depend linearly on $\mathcal{V}_o$:

$$\phi(x,t) = \phi_0^{(0)} + \mathcal{V}_o \phi_1^{(1)}(x) \mathrm{e}^{\mathrm{i}\omega t}, \tag{5a}$$

$$n_r(x,t) = n_0^{(0)} + \mathcal{V}_o n_{r,1}^{(1)}(x) \mathrm{e}^{\mathrm{i}\omega t}, \tag{5b}$$

where $\mathcal{V}_o \phi_1^{(1)}$ and $\mathcal{V}_o n_{r,1}^{(1)}$ are complex valued $O(\mathcal{V}_o)$ perturbations. Here, we assume that the electrodes do not carry a "native" surface charge; hence, the equilibrium potential is $\phi_0^{(0)} = 0$, and the equilibrium ion density is uniform, $n_0^{(0)} = 1$. In (5), the notation is that the numerical subscripts and parenthetic superscripts indicate to which harmonic and which order of voltage the quantity corresponds, respectively. The harmonics in (5) are 0 - steady and 1 - first, or fundamental. While this is evident in (5) we explicitly state it here to be consistent with later notation.

This approach works because at $O(\mathcal{V}_o)$ the nonlinear term in (3b) degenerates to a coupling of $\mathcal{V}_o \phi_1^{(1)}$ with $n_0^{(0)}$ and oscillates at $\mathrm{e}^{\mathrm{i}\omega t}$. More specifically, as long as $O(\mathcal{V}_o^2)$ terms can be neglected, there is no multiplication of complex functions and only terms oscillating at $\mathrm{e}^{\mathrm{i}\omega t}$ will be present. Here, the real part is the physically meaningful portion since the applied voltage is $\mathcal{V}_o \cos(\omega t)$. When $O(\mathcal{V}_o^2)$ terms cannot be neglected, the coupling of complex functions (e.g., $\phi_1^{(1)} \mathrm{e}^{\mathrm{i}\omega t}$ and $n_{r,1}^{(1)} \mathrm{e}^{\mathrm{i}\omega t}$) manifests as additional harmonic modes in the electrolyte response.

At $O(\mathcal{V}_o)$, the fundamental mode (first harmonic) dominates the overall response but as $\mathcal{V}_o$ increases, the higher order harmonics need to be taken into account. The solution for this oscillating system can therefore be written as a Fourier series, which for $g(x,t) = \phi(x,t)$ or $n_r(x,t)$ is

$$g(x,t) = a_0(x) + \sum_{k=1}^{\infty} a_k(x) \cos(k\omega t) + b_k(x) \sin(k\omega t), \tag{6}$$

where a_k and b_k are real functions of ω. Here, a_0 is just the stationary ($k = 0$) contribution. Equation (6) can be rewritten using complex functions via Euler's formula, $\mathrm{e}^{\mathrm{i}z} = \cos(z) + \mathrm{i}\sin(z)$. The result is a complex Fourier series,

$$g(x,t) = a_0(x) + \sum_{k=1}^{\infty} A_k(x) \mathrm{e}^{k\mathrm{i}\omega t} + B_k(x) \mathrm{e}^{-k\mathrm{i}\omega t}, \tag{7}$$

where $A_k = (a_k - \mathrm{i}b_k)/2$ and $B_k = (a_k + \mathrm{i}b_k)/2$ are complex conjugates. Note that the sum in (7) is of complex conjugates and is therefore real valued. Thus, we can express the solutions to (3) as

$$\phi(x,t) = \phi_0(x) + \sum_{k=1}^{\infty} \phi_k(x) \mathrm{e}^{k\mathrm{i}\omega t} + \phi_{-k}(x) \mathrm{e}^{-k\mathrm{i}\omega t}, \tag{8a}$$

$$n_r(x,t) = n_{r,0}(x) + \sum_{k=1}^{\infty} n_{r,k}(x) \mathrm{e}^{k\mathrm{i}\omega t} + n_{r,-k}(x) \mathrm{e}^{-k\mathrm{i}\omega t}, \tag{8b}$$

where the "coefficients", ϕ_k and $n_{r,k}$, are complex valued functions of ω while ϕ_0 and $n_{r,0}$ are real valued. A negative subscript ($-k$) denotes the complex conjugate of the corresponding positive subscript (k), and the dependence on $\mathcal{V}_o$ is implicit in the coefficients.

Substitution of (8) into (3) yields an infinite set of coupled nonlinear ordinary differential equations. Without giving the full expression, we can address the primary difficulty of the resulting set of equations. The nonlinear term in (3b) ($n_r \partial\phi/\partial x$) results in doubly infinite sums through the coupling of terms containing $\mathrm{e}^{k\mathrm{i}\omega t}$ with $\mathrm{e}^{-q\mathrm{i}\omega t}$ where k and q are any positive integers. The result is terms which look like

$$\sum_{k=1}^{\infty} \sum_{q=1}^{\infty} n_{r,k+q} \phi_{-q} \mathrm{e}^{k\mathrm{i}\omega t} + \sum_{q=1}^{\infty} n_{r,q} \phi_{-q}, \tag{9}$$

for example. This arises due to the fact that there are an infinite number of positive integers k and q such that $(k+q) - q = k$ and $q + (-q) = 0$. Hence, the k^{th} harmonic is dependent upon *all* other harmonic modes q, even those for which $q > k$. The series must therefore be truncated

at a suitable harmonic. We can alleviate ourselves of the doubly infinite sums by expressing the Fourier coefficients ϕ_k and $n_{r,k}$ as power series in $\mathcal{V}_o$. We give the form of the power series later but it is instructive to first demonstrate how it arises from the nonlinearity of (3b).

First, ϕ_k and $n_{r,k}$ contain a linear dependence on $\mathcal{V}_o$ from (5) which we denote as $\phi_1^{(1)}$ and $n_{r,1}^{(1)}$. Recall that a parenthetic superscript indicates the order of $\mathcal{V}_o$ the quantity applies to. The coupling of $\mathcal{V}_o n_{r,1}^{(1)} \mathrm{e}^{\mathrm{i}\omega t}$ with $\mathcal{V}_o \phi_1^{(1)} \mathrm{e}^{\mathrm{i}\omega t}$ produces terms which are $O(\mathcal{V}_o^2)$ and oscillate at the second harmonic, $\mathrm{e}^{2\mathrm{i}\omega t}$. We also obtain the corresponding complex conjugates. Furthermore, the coupling of $\mathcal{V}_o n_{r,1}^{(1)} \mathrm{e}^{\mathrm{i}\omega t}$ with $\mathcal{V}_o \phi_{-1}^{(1)} \mathrm{e}^{-\mathrm{i}\omega t}$ also results in $O(\mathcal{V}_o^2)$ terms but they are non-oscillatory, or stationary. The $O(\mathcal{V}_o^2)$ terms for ϕ (and similarly for n_r) are thus $\mathcal{V}_o^2 \phi_2^{(2)} \mathrm{e}^{2\mathrm{i}\omega t}$, $\mathcal{V}_o^2 \phi_{-2}^{(2)} \mathrm{e}^{-2\mathrm{i}\omega t}$, and $\mathcal{V}_o^2 \phi_0^{(2)}$. These terms are coupled to other $O(\mathcal{V}_o^2)$ terms but also to $O(\mathcal{V}_o)$ and $O(1)$ terms. Coupling with $O(\mathcal{V}_o)$ yields terms which are $O(\mathcal{V}_o^3)$ and oscillate at $\mathrm{e}^{3\mathrm{i}\omega t}$ and $\mathrm{e}^{\mathrm{i}\omega t}$ (through coupling with a term oscillating at $\mathrm{e}^{-\mathrm{i}\omega t}$). As we show later, $O(\mathcal{V}_o^3)$ is the first nonlinear contribution to the current. Thus, we truncate our series here and write the expansions as

$$\begin{aligned}\phi(x,t) = \phi_0^{(0)} &+ \mathcal{V}_o \left(\phi_1^{(1)} \mathrm{e}^{\mathrm{i}\omega t} + \phi_{-1}^{(1)} \mathrm{e}^{-\mathrm{i}\omega t}\right) \\ &+ \mathcal{V}_o^2 \left(\phi_2^{(2)} \mathrm{e}^{2\mathrm{i}\omega t} + \phi_0^{(2)} + \phi_{-2}^{(2)} \mathrm{e}^{-2\mathrm{i}\omega t}\right) \\ &+ \mathcal{V}_o^3 \Big(\phi_3^{(3)} \mathrm{e}^{3\mathrm{i}\omega t} + \phi_1^{(3)} \mathrm{e}^{\mathrm{i}\omega t} \\ &\qquad + \phi_{-1}^{(3)} \mathrm{e}^{-\mathrm{i}\omega t} + \phi_{-3}^{(3)} \mathrm{e}^{-3\mathrm{i}\omega t}\Big) \\ &+ O\left(\mathcal{V}_o^4\right),\end{aligned} \tag{10a}$$

and

$$\begin{aligned}n_r(x,t) = n_{r,0}^{(0)} &+ \mathcal{V}_o \left(n_{r,1}^{(1)} \mathrm{e}^{\mathrm{i}\omega t} + n_{r,-1}^{(1)} \mathrm{e}^{-\mathrm{i}\omega t}\right) \\ &+ \mathcal{V}_o^2 \left(n_{r,2}^{(2)} \mathrm{e}^{2\mathrm{i}\omega t} + n_{r,0}^{(2)} + n_{r,-2}^{(2)} \mathrm{e}^{-2\mathrm{i}\omega t}\right) \\ &+ \mathcal{V}_o^3 \Big(n_{r,3}^{(3)} \mathrm{e}^{3\mathrm{i}\omega t} + n_{r,1}^{(3)} \mathrm{e}^{\mathrm{i}\omega t} \\ &\qquad + n_{r,-1}^{(3)} \mathrm{e}^{-\mathrm{i}\omega t} + n_{r,-3}^{(3)} \mathrm{e}^{-3\mathrm{i}\omega t}\Big) \\ &+ O\left(\mathcal{V}_o^4\right),\end{aligned} \tag{10b}$$

which can be rearranged to show how the Fourier coefficients in (8) depend on voltage. For example, for the potential from (10a),

$$\phi_0(x) = \phi_0^{(0)} + \mathcal{V}_o^2 \phi_0^{(2)} + \mathcal{V}_o^4 \phi_0^{(4)} + \cdots, \tag{11a}$$

$$\phi_1(x) = \mathcal{V}_o \phi_1^{(1)} + \mathcal{V}_o^3 \phi_1^{(3)} + \mathcal{V}_o^5 \phi_1^{(5)} + \cdots, \tag{11b}$$

$$\phi_2(x) = \mathcal{V}_o^2 \phi_2^{(2)} + \mathcal{V}_o^4 \phi_2^{(4)} + \mathcal{V}_o^6 \phi_2^{(6)} + \cdots, \tag{11c}$$

etc, where $\phi_0^{(0)} = 0$. The power series can more generally be written as

$$\phi_k(x) = \sum_{v=0}^{\infty} \phi_k^{(2v+k)}(x) \mathcal{V}_o^{2v+k}, \tag{12a}$$

$$\phi_{-k}(x) = \sum_{v=0}^{\infty} \phi_{-k}^{(2v+k)}(x) \mathcal{V}_o^{2v+k}, \tag{12b}$$

and an analogous series for the ion densities, $n_{r,\pm k}$. The moderately nonlinear expansions (10) can be written concisely as

$$\phi(x,t) = \phi_0^{(0)} + \sum_{v=1}^{\infty} \mathcal{V}_o^v \left(\sum_{l=0}^{v} \phi_{v-2l}^{(v)} \mathrm{e}^{(v-2l)\mathrm{i}\omega t}\right), \tag{13a}$$

$$n_r(x,t) = n_{r,0}^{(0)} + \sum_{v=1}^{\infty} \mathcal{V}_o^v \left(\sum_{l=0}^{v} n_{r,v-2l}^{(v)} \mathrm{e}^{(v-2l)\mathrm{i}\omega t}\right). \tag{13b}$$

From the pattern in (10), or equivalently the series in (13), it is apparent that the odd orders of voltage contain only odd harmonics while the even orders of voltage contain only even harmonics. Note that the sums in (10) are all real valued since a complex quantity is always present with its complex conjugate. Also, note that the stationary terms are always real valued quantities.

Substitution of (13) into (3) yields a set of *linear* differential equations. We present here the explicit statements of the governing equations up to $O(\mathcal{V}_o^3)$ for $\mathrm{e}^{k\mathrm{i}\omega t}$, where $k \geq 0$. The equations for $k < 0$ are obtained by taking the complex conjugate. The resulting $O(\mathcal{V}_o)$ equations for $\mathrm{e}^{\mathrm{i}\omega t}$ are

$$\frac{\mathrm{d}^2 \phi_1^1}{\mathrm{d}x^2} = -\frac{n_{+,1}^{(1)} - n_{-,1}^{(1)}}{2\epsilon^2}, \tag{14a}$$

$$\frac{\mathrm{d}^2 n_{r,1}^{(1)}}{\mathrm{d}x^2} = \frac{\mathrm{i}\omega}{\epsilon} n_{r,1}^{(1)} - r\left[n_0^{(0)} \frac{\mathrm{d}^2 \phi_1^{(1)}}{\mathrm{d}x^2}\right], \tag{14b}$$

$$\frac{\mathrm{d}n_{r,1}^{(1)}}{\mathrm{d}x} + r\left[n_0^{(0)} \frac{\mathrm{d}\phi_1^{(1)}}{\mathrm{d}x}\right] = 0, \text{ at } x = \pm 1 \tag{14c}$$

$$\phi_1^{(1)} = \pm\frac{1}{2}, \text{ at } x = \pm 1. \tag{14d}$$

The $O(\mathcal{V}_o^2)$ equations have $\mathrm{e}^{2\mathrm{i}\omega t}$ and stationary contributions. The $\mathrm{e}^{2\mathrm{i}\omega t}$ equations are

$$\frac{\mathrm{d}^2 \phi_2^{(2)}}{\mathrm{d}x^2} = -\frac{n_{+,2}^{(2)} - n_{-,2}^{(2)}}{2\epsilon^2}, \tag{15a}$$

$$\frac{\mathrm{d}^2 n_{r,2}^{(2)}}{\mathrm{d}x^2} = \frac{2\mathrm{i}\omega}{\epsilon} n_{r,2}^{(2)} - r\frac{\mathrm{d}}{\mathrm{d}x}\left[n_0^{(0)} \frac{\mathrm{d}\phi_2^{(2)}}{\mathrm{d}x} + F_{r,2}^{(2)}\right], \tag{15b}$$

$$\frac{\mathrm{d}n_{r,2}^{(2)}}{\mathrm{d}x} + r\left[n_0^{(0)} \frac{\mathrm{d}\phi_2^{(2)}}{\mathrm{d}x} + F_{r,2}^{(2)}\right] = 0, \text{ at } x = \pm 1, \tag{15c}$$

$$\phi_2^{(2)} = 0, \text{ at } x = \pm 1, \tag{15d}$$

which are forced by,

$$F_{r,2}^{(2)} = n_{r,1}^{(1)} \frac{\mathrm{d}\phi_1^{(1)}}{\mathrm{d}x}. \tag{15e}$$

The stationary equations are

$$\frac{\mathrm{d}^2\phi_0^{(2)}}{\mathrm{d}x^2} = -\frac{n_{+,0}^{(2)} - n_{-,0}^{(2)}}{2\epsilon^2}, \tag{16a}$$

$$\frac{\mathrm{d}^2 n_{r,0}^{(2)}}{\mathrm{d}x^2} = -r\frac{\mathrm{d}}{\mathrm{d}x}\left[n_0^{(0)}\frac{\mathrm{d}\phi_0^{(2)}}{\mathrm{d}x} + F_{r,0}^{(2)}\right], \tag{16b}$$

$$\frac{\mathrm{d}n_{r,0}^{(2)}}{\mathrm{d}x} + r\left[n_0^{(0)}\frac{\mathrm{d}\phi_0^{(2)}}{\mathrm{d}x} + F_{r,0}^{(2)}\right] = 0, \text{ at } x = \pm 1, \tag{16c}$$

$$\phi_0^{(2)} = 0, \text{ at } x = \pm 1, \tag{16d}$$

which are forced by,

$$F_{r,0}^{(2)} = n_{r,1}^{(1)}\frac{\mathrm{d}\phi_{-1}^{(1)}}{\mathrm{d}x} + n_{r,-1}^{(1)}\frac{\mathrm{d}\phi_1^{(1)}}{\mathrm{d}x}. \tag{16e}$$

The $O(\mathcal{V}_o^3)$ equations contain both $\mathrm{e}^{3\mathrm{i}\omega t}$ and $\mathrm{e}^{\mathrm{i}\omega t}$ contributions. The $\mathrm{e}^{3\mathrm{i}\omega t}$ equations are

$$\frac{\mathrm{d}^2\phi_3^{(3)}}{\mathrm{d}x^2} = -\frac{n_{+,3}^{(3)} - n_{-,3}^{(3)}}{2\epsilon^2}, \tag{17a}$$

$$\frac{\mathrm{d}^2 n_{r,3}^{(3)}}{\mathrm{d}x^2} = \frac{3\mathrm{i}\omega}{\epsilon}n_{r,3}^{(3)} - r\frac{\mathrm{d}}{\mathrm{d}x}\left[n_0^{(0)}\frac{\mathrm{d}\phi_3^{(3)}}{\mathrm{d}x} + F_{r,3}^{(3)}\right], \tag{17b}$$

$$\frac{\mathrm{d}n_{r,3}^{(3)}}{\mathrm{d}x} + r\left[n_0^{(0)}\frac{\mathrm{d}\phi_3^{(3)}}{\mathrm{d}x} + F_{r,3}^{(3)}\right] = 0, \text{ at } x = \pm 1, \tag{17c}$$

$$\phi_3^{(3)} = 0, \text{ at } x = \pm 1, \tag{17d}$$

which are forced by,

$$F_{r,3}^{(3)} = n_{r,1}^{(1)}\frac{\mathrm{d}\phi_2^{(2)}}{\mathrm{d}x} + n_{r,2}^{(2)}\frac{\mathrm{d}\phi_1^{(1)}}{\mathrm{d}x}, \tag{17e}$$

and the $\mathrm{e}^{\mathrm{i}\omega t}$ equations are

$$\frac{\mathrm{d}^2\phi_1^{(3)}}{\mathrm{d}x^2} = -\frac{n_{+,1}^{3} - n_{-,1}^{3}}{2\epsilon^2}, \tag{18a}$$

$$\frac{\mathrm{d}^2 n_{r,1}^{3}}{\mathrm{d}x^2} = \frac{\mathrm{i}\omega}{\epsilon}n_{r,1}^{(3)} - r\frac{\mathrm{d}}{\mathrm{d}x}\left[n_0^{(0)}\frac{\mathrm{d}\phi_1^{(3)}}{\mathrm{d}x} + F_{r,1}^{(3)}\right], \tag{18b}$$

$$\frac{\mathrm{d}n_{r,1}^{(3)}}{\mathrm{d}x} + r\left[n_0^{(0)}\frac{\mathrm{d}\phi_1^{(3)}}{\mathrm{d}x} + F_{r,3}^{(3)}\right] = 0, \text{ at } x = \pm 1, \tag{18c}$$

$$\phi_1^{(3)} = 0, \text{ at } x = \pm 1, \tag{18d}$$

which are forced by,

$$F_{r,1}^{(3)} = n_{r,1}^{(1)}\frac{\mathrm{d}\phi_0^{(2)}}{\mathrm{d}x} + n_{r,-1}^{(1)}\frac{\mathrm{d}\phi_2^{(2)}}{\mathrm{d}x} + n_{r,2}^{(2)}\frac{\mathrm{d}\phi_{-1}^{(1)}}{\mathrm{d}x} + n_{r,0}^{(2)}\frac{\mathrm{d}\phi_1^{(1)}}{\mathrm{d}x}. \tag{18e}$$

The no-flux boundary conditions (14c), (15c), (16c), (17c), and (18c) are equivalent to the statement that the total number of ions at any order of voltage remains constant. Mathematically, this takes the form

$$\int_{-1}^{1} n_{r,k}^{(v)}\mathrm{d}x = \begin{cases} 2 & ; v = 0 \\ 0 & ; v \geq 1, \end{cases} \tag{19}$$

where v is the order of voltage. This form of the no-flux condition is needed to solve equations (16) since the governing equations (16b) are the derivatives of the boundary conditions (16c). Thus one of the boundary conditions (16c) are redundant. Reformulating (16c) into (19), it is possible to derive a new set of governing equations for the stationary $O(\mathcal{V}_o^2)$ terms:

$$\epsilon^2\frac{\mathrm{d}^2\phi_0^{(2)}}{\mathrm{d}x^2} = \phi_0^{(2)} + \frac{1}{2}(\mathcal{I}_+ + \mathcal{I}_-) - \frac{1}{2}\int_{-1}^{1}\phi_0^{(2)}\mathrm{d}x - \frac{1}{4}\int_{-1}^{1}(\mathcal{I}_+ + \mathcal{I}_-)\,\mathrm{d}x, \tag{20a}$$

$$n_{r,0}^{(2)} = -r\phi_0^{(2)} - r\mathcal{I}_r + r\frac{1}{2}\int_{-1}^{1}\phi_0^{(2)}\mathrm{d}x + r\frac{1}{2}\int_{-1}^{1}\mathcal{I}_r\mathrm{d}x, \tag{20b}$$

where,

$$\mathcal{I}_r = \int_{-1}^{x} F_{r,0}^{(2)}\mathrm{d}\bar{x}, \tag{20c}$$

This set of equations has thus been reduced to a single integro-differential equation (20a) for $\phi_0^{(2)}$. Once (20a) is solved, $n_{r,0}^{(2)}$ is easily computed from $\phi_0^{(2)}$.

Thus far we have claimed that the electrolyte dynamics are linear so long as $\mathcal{V}_o < 1$, while for $\mathcal{V}_o > 1$ the response is voltage dependent. This is not precisely the case, though $\mathcal{V}_o < 1$ does ensure linearity. We can obtain a useful frequency-dependent criteria for linearity by considering the linear ion density perturbation $\mathcal{V}_o n_{r,1}^{(1)}$ from (5). When $\mathcal{V}_o|n_{r,1}^{(1)}| \ll n_0^{(0)}$, the nonlinear term in (3b) can be linearized since $n_r \approx n_0^{(0)}$. Physically, this means that the extent of the ion motion is sufficiently small that the perturbation to the equilibrium distribution is negligible. From the analytic solutions obtained by substitution of (5) into (3), it can be shown that the above inequality is satisfied when[26]

$$\mathcal{V}_o \ll \mathcal{V}_c = \left|\frac{1}{\beta^2} + \frac{\mathrm{i}\omega}{\beta}\coth\left(\frac{\beta}{\epsilon}\right)\right|, \tag{21}$$

where $\beta = \sqrt{1 + \mathrm{i}\omega\epsilon}$. This gives a frequency-voltage relationship for linearity where, for a given ω, the ion perturbation is small if $\mathcal{V}_o$ is less than the critical voltage, $\mathcal{V}_c$.

Figure 2 is a plot of the dimensionless applied voltage in excess of the thermal voltage, $\mathcal{V}_o - 1$, against ω with

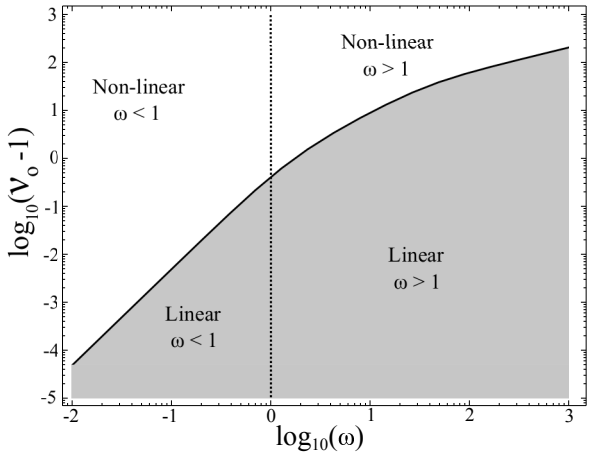

FIG. 2: Plot of voltage amplitude in excess of thermal voltage, $\mathcal{V}_o - 1$, versus the driving frequency, ω. The solid line is the critical voltage $\mathcal{V}_c$ for linearity predicted by (21) and the dotted line indicates the RC frequency. As the driving frequency increases, a larger voltage amplitude is required to yield a nonlinear response.

the linear and nonlinear regions separated by the solid line created by $\mathcal{V}_c$. The vertical dotted line separates the plot into frequencies above or below the RC frequency. It is clear that $\mathcal{V}_o \leq 1$ always results in a linear response, and as frequency increases, the voltage needed to observe nonlinear effects increases.

The physical effect of increasing frequency can be understood in terms of ion motion. At low frequencies, the ions have time to move in response to the applied voltage and begin to form Debye layers at the electrode surfaces. The developing Debye layers are what ultimately give rise to the nonlinearities in the charge dynamics. As the frequency increases, the ions are only able to move a short distance before the voltage has reversed and they must move in the opposite direction, precluding the formation of Debye layers. Therefore, although there is a greater driving force at large $\mathcal{V}_o$, there exists a frequency beyond which the dynamics will be linear in $\mathcal{V}_o$.

Equations (14), (15), and (17)-(20) were solved using the MATLAB bvp4c solver. It is a finite difference scheme utilizing the three stage Lobatto 3a collocation method.

III. RESULTS

A. Harmonic Profiles

We begin with general observations regarding the electrostatic potential and ion densities that will aid subsequent analysis. First, at $O(\mathcal{V}_o)$ and $O(\mathcal{V}_o^3)$, the ion densities are equal and opposite (e.g. $n_{+,1}^{(1)} = -n_{-,1}^{(1)}$) (figure 3a and 3e). This is not surprising since the electrolyte is symmetric with equal ionic diffusivities. A consequence of this behavior is that the ion densities for odd orders of voltage are anti-symmetric about $x = 0$.

The second, more interesting, observation is that the ion densities and electrostatic potential for $O(\mathcal{V}_o^2)$ are not only symmetric, but also $\phi_2^{(2)} = \phi_0^{(2)} = 0$, $n_{+,2}^{(2)} = n_{-,2}^{(2)}$, and $n_{+,0}^{(2)} = n_{-,0}^{(2)}$ (figure 3b and 3c). At this order, the voltage on the electrode is "squared" which leads to an identical charge on each and no electric field in the electrolyte. However, the ions still migrate due to the electromigrative forcing originating from the $O(\mathcal{V}_o)$ dynamics, $F_{r,2}^{(2)} = n_{r,1}^{(1)} \mathrm{d}\phi_1^{(1)}/\mathrm{d}x$. This symmetric motion corresponds to the adsorption of neutral salt (total ion concentration) leading to a depletion of neutral salt in the bulk electrolyte as can be seen in figures 3b and 3c.

Olesen *et al.* [27] predicted this adsorption of salt in the context of a "strongly nonlinear" regime in which oscillating diffusion layers could almost completely deplete the salt concentration outside the Debye layers. They referred to this effect as "AC capacitive desalination." Remarkably, they showed that despite the oscillatory nature of the driving voltage, there is a time-averaged salt adsorption into the Debye layers. We demonstrate that this "steady" desalination of the bulk electrolyte also occurs at moderately large voltages. Our analysis indicates neutral salt adsorption occurs first at $O(\mathcal{V}_o^2)$ and, in general, at all even orders of voltage.

B. Nonlinear Current

We now calculate the overall current through the system, $I(t) = \mathrm{d}Q/\mathrm{d}t$, where Q is the total charge on the electrode surface normalized by $A\varepsilon k_B T/eL$, where A is the surface area of the electrode in contact with electrolyte. Using Gauss's law, $I(t)$ can be related to ϕ, and the dimensionless current (normalized by $A\varepsilon D k_B T/e\lambda_D L^2$) is $I(t) = -\partial^2\phi/\partial x \partial t|_{x=-1}$[31]. The current can be expanded in the same form as (10) where it is clear from the above explanation that the $O(\mathcal{V}_o^2)$ contribution is zero since $\phi_k^{(2)} = 0$. In fact, the stationary term $\phi_0^{(2)}$ cannot contribute to the current regardless of electrolyte symmetry since it lacks a time dependent co-factor (see (10)). More generally, for a symmetric electrolyte, all even orders of voltage will have zero electrostatic potential and be non-contributing to the overall current.

The relationship between current and voltage can be visualized from a Lissajous plot, which is a parametric mapping of current versus voltage, each normalized by their respective maximums. The more closely the resulting curve resembles a line, the more in-phase the current and voltage are. Likewise, a perfectly out-of-phase (but linear in $\mathcal{V}_o$) current results in a circular curve. Physically, the out-of-phase circular curves are achieved through the capacitance of either the Debye lay-

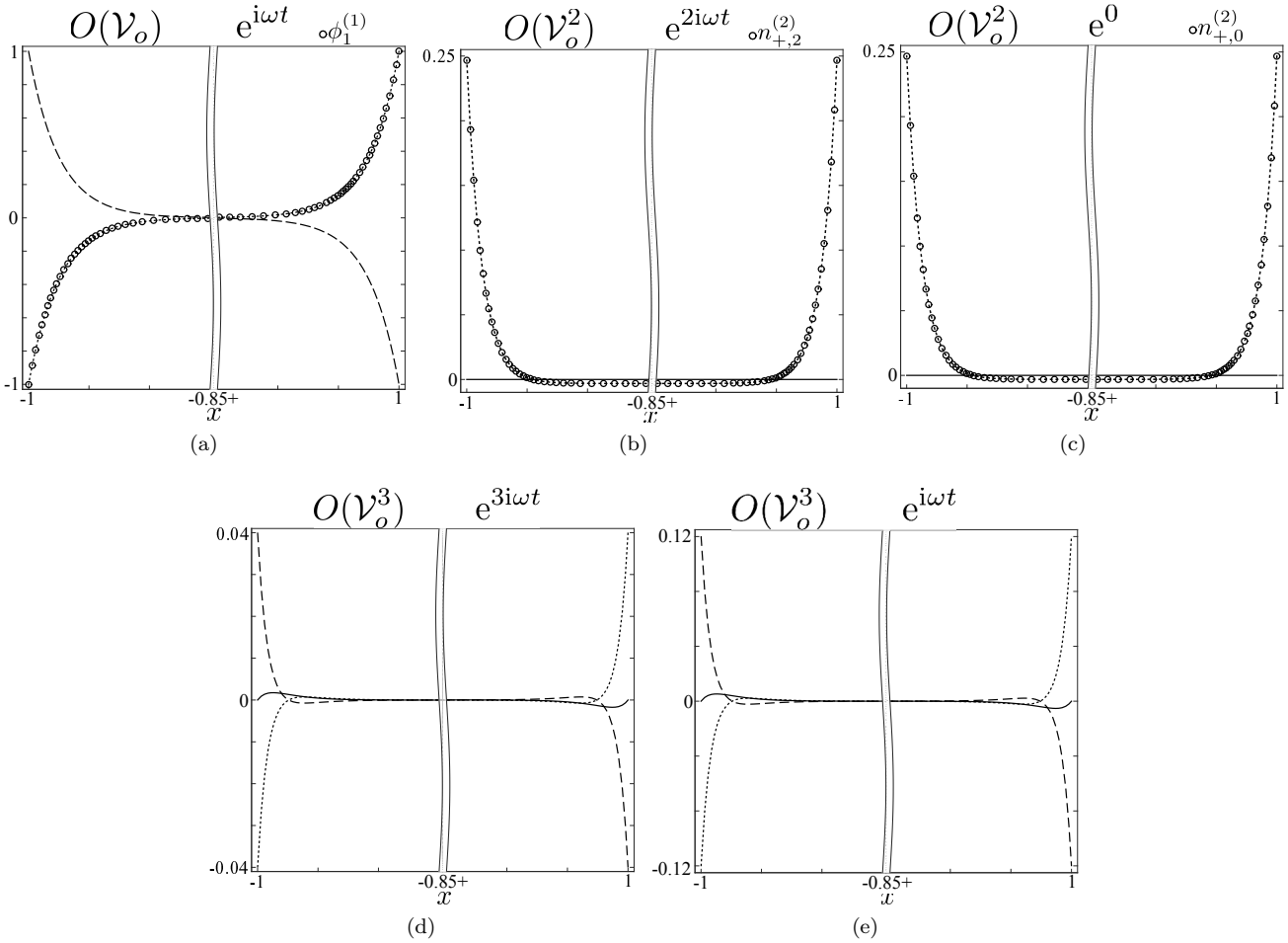

FIG. 3: Total individual harmonic modes of electrostatic potential (solid line), positive ion density (dashed line), and negative ion density (dotted line) for $\omega = 0.01$, $\epsilon = 0.025$, and $t = 0$ throughout the cell. Symbols in (a)-(c) are used to show data that is hidden behind other lines; they indicate electrostatic potential (a), positive ion density (b) and (c). The odd harmonics (a), (d), and (e) are anti-symmetric about $x = 0$ and the ion densities are equal and opposite. In (a), the dimensionless negative ion density is equal to the electrostatic potential. The even harmonics (b) and (c) are symmetric and the ion densities are equal due to the symmetry of the electrolyte. An interesting result of this symmetry is that the even harmonics of the potential are uniformly zero.

ers ($\omega \ll 1$) or the dielectric solvent ($\omega \gg 1$) and the most in-phase curves represent a relative balance between conduction of ions and capacitive charging ($\omega \sim 1$).

Using the idea of Pipkin diagrams from rheology[32], we make a diagram of Lissajous plots for a range of voltages and frequencies (figure 4 for $\epsilon = 0.025$ and figure 5 for $\epsilon = 0.25$). The axes on each individual Lissajous plot range from -1 to 1 while the axes values for the total diagram are explicitly labeled. The solid and dashed lines are results from our moderately nonlinear expansion (10) and, for comparison, a full numerical solution to the PNP equations, respectively. (Numerical solution obtained using a finite difference method via the MATLAB pdepe solver.) The color is a visual measure of the linearity of the response:

$$f = \left[\frac{\int_0^{T/2} \left(I^{(1)} \right)^2 \mathrm{d}t}{\int_0^{T/2} \left(I^{(1)} + \mathcal{V}_o^2 I^{(3)} \right)^2 \mathrm{d}t} \right]^{1/2}, \qquad (22)$$

where $T = 2\pi/\omega$ is the period of oscillation. For $0.9 < f \leq 1$, the response is primarily linear and the resulting Lissajous plot is circular at low and high frequencies; becoming ellipitcal at moderate frequencies. Nonlinear response is signified by a distortion of the Lissajous plot from circular or elliptical - especially at low frequencies. The lowest value for f in figure 4 is 0.53. Including higher order terms in voltage and frequency would likely reduce this value further so it is a conservative measure of linearity.

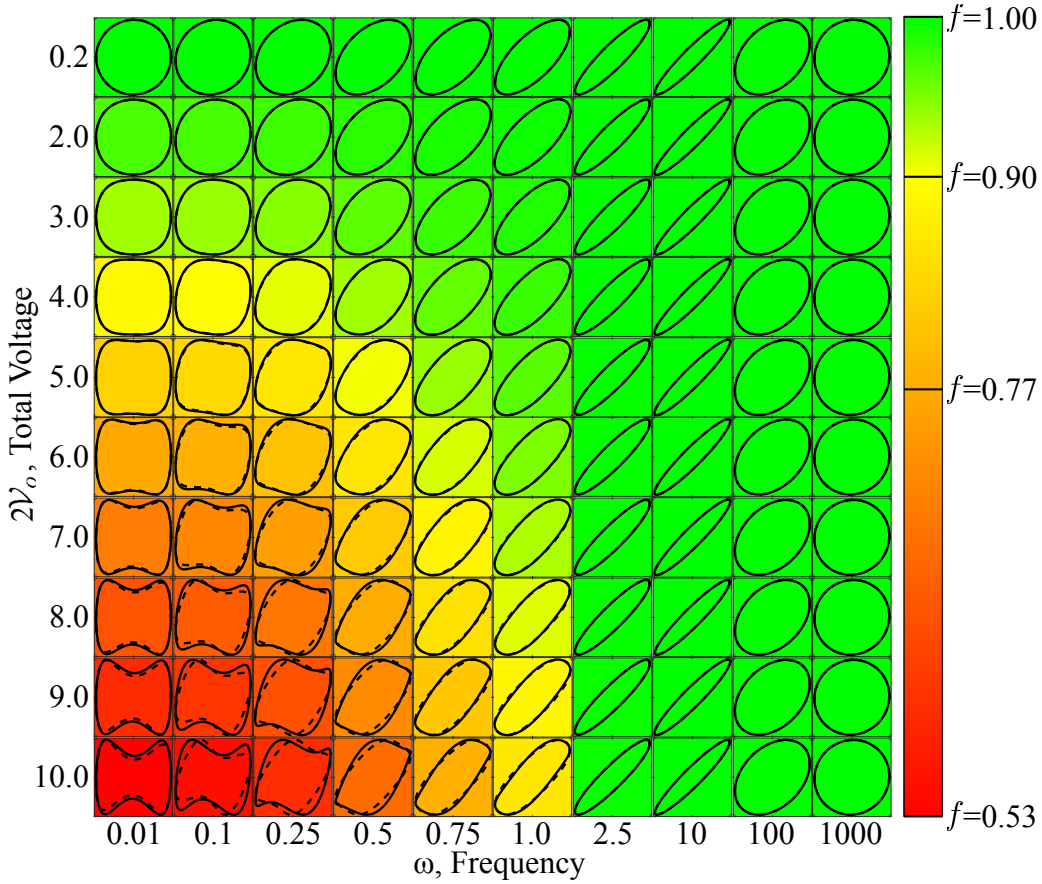

FIG. 4: (Color online) Pipkin diagram for $\epsilon = 0.025$. On each plot, the horizontal axis is voltage and the vertical axis is current, both scaled to be in the range [-1, 1]. The solid lines are the result from our moderately nonlinear expansion and the dashed lines are numerical solutions to the PNP equations. The frequency, ω, increases to the right and the total applied voltage difference increases down. Linear response dominates at low voltages and for frequencies $\omega > 1$. As the conditions approach the lower left portion of the figure, the Lissajous curve distorts from the elliptical shape typical of linear response. The color is based upon the linearity fraction, f, defined in equation (22) with two distinct regions: f=[1, 0.9] the color changes from green to yellow; f=[0.9, 0.53] the color changes from yellow to red and a linear theory captures relatively little of the dynamics. Also labeled on the color bar is $f = 0.77$, which is the value corresponding to $2\mathcal{V}_o = 6$ and $\omega = 0.01$.

Most apparent from figure 4 is that the responses which are most nonlinear are those at high voltages and low frequencies. This is not surprising given the relationship between ω and $\mathcal{V}_o$ in (21) for linear response (see also figure 2). What is notable about figure 4 is it suggests the current response is essentially linear for $\omega > 1$. This could allow use of linearizing approximations and traditional models of EIS even for large driving voltages. Using large voltages would be advantageous for eliminating noise in measurements of current.

Regarding the validity of our moderately nonlinear expansions (10), we see excellent agreement with the full numerical solution for all ω up to $2\mathcal{V}_o = 6$ and for all $\omega > 1$ for $2\mathcal{V}_o > 6$, where $f = 0.77$ in the former and the dynamics are predominately linear in the latter. For $2\mathcal{V}_o > 6$ and $\omega < 1$, we still capture the qualitative features of the current. This highlights the usefulness of (10) in describing a moderately nonlinear response.

For comparison with the above thin Debye layer ($\epsilon = 0.025$) diagram, figure 5 is a Pipkin diagram for $\epsilon = 0.25$. The coloring scheme and scale is identical to the one used in figure 4. Once again, the most nonlinear response is seen for low frequencies at high voltages and becomes more linear as frequency increases. One significant difference is the linearity factor (22) suggests the response is more linear for all values of $\mathcal{V}_o$ plotted since $f > 0.82$. Comparing the full numerical solutions for $\omega = 0.01$, we conclude that the same voltage of $2\mathcal{V}_o = 6$ is the largest voltage amplitude for which our expansion has good agreement. Here, it corresponds to $f = 0.93$, compared with $f = 0.77$ for $\epsilon = 0.025$. The Lissajous plots are also hexagon-like in shape at large voltages which

contrasts to the "bow-tie"-like shape for $\epsilon = 0.025$. The apparent lack of this feature in our perturbation analysis suggests more terms in the voltage expansion are needed as ϵ increases. Another difference is that for $\epsilon = 0.25$, the plots are generally more circular than the corresponding plot for $\epsilon = 0.025$. This is a direct consequence of there being fewer ions in the electrolyte and hence less in-phase conduction. Alternatively, the thicker Debye cloud at larger ϵ results in a diminished frequency gap between the capacitive response due to the dielectric solvent and the Debye layer.

To better understand how higher order harmonics (specifically the third harmonic) effect the current, figure 6 shows how the current response changes with frequency for a linear ($\mathcal{V}_o = 0.1$, solid) and moderately nonlinear ($\mathcal{V}_o = 3$, dashed) voltage amplitude. The presence of the third harmonic, $e^{3i\omega t}$, is readily apparent in figure 6 for $\omega = 0.01$ and results in a "double-peak" in the current versus time plot and a "bow-tie" in the Lissajous plot. Also apparent is the lack of a second harmonic which if non-zero would reduce the size of the second peak.

As the frequency increases, the current shifts to be more in-phase with the applied voltage and the second peak starts to diminish. The phase shift is due to a reduction in Debye layer capacitance resulting in a relative increase in in-phase conduction (see explanation for (21)). The second peak results from the third harmonic and as ω approaches 1 from low values, higher order harmonics ($\phi_1^{(3)}$, $\phi_3^{(3)}$, etc.) become less prominent. That is, they decrease in amplitude relative to $\phi_1^{(1)}$. Since the second peak is due entirely to the third harmonic, this necessarily leads to it vanishing. As it diminishes, the nonlinear current more closely resembles that of the linear response. The second peak could also be reduced by the existence of a second harmonic in the case of asymmetric electrolytes, but $\phi_2^{(2)} = 0$ is guaranteed for symmetric, point-like electrolytes. Even if $\phi_2^{(2)} \neq 0$, it would also diminish in amplitude as ω increases.

Therefore, linear dynamics can result at high voltages because the higher order harmonic modes decrease in amplitude as frequency increases. This results in a reduction in the extent of ion motion and less capacitive storing in Debye layers. Since the nonlinear response is a direct consequence of the capacitive storing, the result is increased linearity in the current response.

Interestingly, the ion densities predicted in figure 3 could lead to unphysical values at sufficiently large $\mathcal{V}_o$ even though each term in (10) is correct, as we show in figure 7. It is a plot of total cation density for a small voltage ($\mathcal{V}_o = 0.1$) and two larger voltages ($\mathcal{V}_o = 1$ and 2) at $\omega = 0.01$ and $t = 0$. For $\mathcal{V}_o = 0.1$, the ion perturbation is primarily due to $O(\mathcal{V}_o)$ effects and is thus antisymmetric. For $\mathcal{V}_o = 1$, the total perturbation is unequal due to the symmetric $O(\mathcal{V}_o^2)$ contribution, giving rise to an increased density of cations on the negative electrode ($x = -1$) compared to the smaller decrease in density on the positive electrode ($x = 1$). For $\mathcal{V}_o = 2$, the asymmetric $O(\mathcal{V}_o^3)$ perturbation is now prevalent enough to significantly affect the ion densities. As a consequence, the positive electrode has a negative density of cations at its surface. It is clearly not physically possible to have negative ion concentrations; however, this does not mean our approach is incorrect. Again, we emphasize that the individual contributions in figure 3 are correct. We use a regular perturbation expansion in $\mathcal{V}_o$ which is asymptotic as $\mathcal{V}_o \to 0$ so it is expected to break down at some $\mathcal{V}_o$ greater than unity. In this view, it is remarkable that the predicted current responses in figure 4 agree well with numerics at $\mathcal{V}_o = 3$ and $\omega = 0.01$ (and even at larger voltages, as explained above).

IV. WEAKLY NONLINEAR IMPEDANCE

Electrochemical impedance spectroscopy (EIS) uses an experimental system such as figure 1 where the electrodes are sufficiently close such that the charge transport occurs primarily normal to the electrode surface. A time varying voltage, $V(t) = \mathcal{V}_o \cos(\omega t)$, is imposed resulting in the charging/discharging of the Debye layers and a current response, $I(t)$. Provided that $\lambda_D \ll L$, the system is analogous to an equivalent circuit in which the two Debye layers are described as capacitors in series with the electrolyte resistance and in parallel is the geometric capacitance of the cell itself via the dielectric solvent.

It is convenient to express the voltage and current as complex quantities: $V(t) = \mathcal{V}_o e^{i\omega t}$ and $I(t) = I_1^{(1)} e^{i\omega t}$. Then the impedance for a symmetric binary electrolyte, defined as $Z = V(t)/I(t)$, is given by[26]

$$Z = \frac{-2\epsilon}{\beta^2 \omega^2} \left[\frac{\mathrm{i}}{\beta} \tanh\left(\frac{\beta}{\epsilon}\right) - \omega \right], \tag{23}$$

where $\beta = \sqrt{1 + \mathrm{i}\omega\epsilon}$. Equation (23) can be used to determine physical properties of the electrolyte such as conductivity and dielectric permittivity by determining the limiting behavior of the real and imaginary components at small and large frequencies[24, 25].

Equation (23) is formally valid when $\mathcal{V}_o \ll \mathcal{V}_c$, i.e. linear response. When this condition is violated, higher order harmonic modes must be included in the expression for $I(t)$. The result is a time dependent "impedance," if defined by simply dividing the voltage by the current. Alternatively, following Olesen *et al.* [27], we define a generalized impedance,

$$\mathcal{Z} = \frac{\int_0^T V(t) e^{-i\omega t} dt}{\int_0^T I(t) e^{-i\omega t} dt}, \tag{24}$$

to capture only those contributions to the current oscillating at the applied frequency. Hence, $\mathcal{Z}$ is time independent.

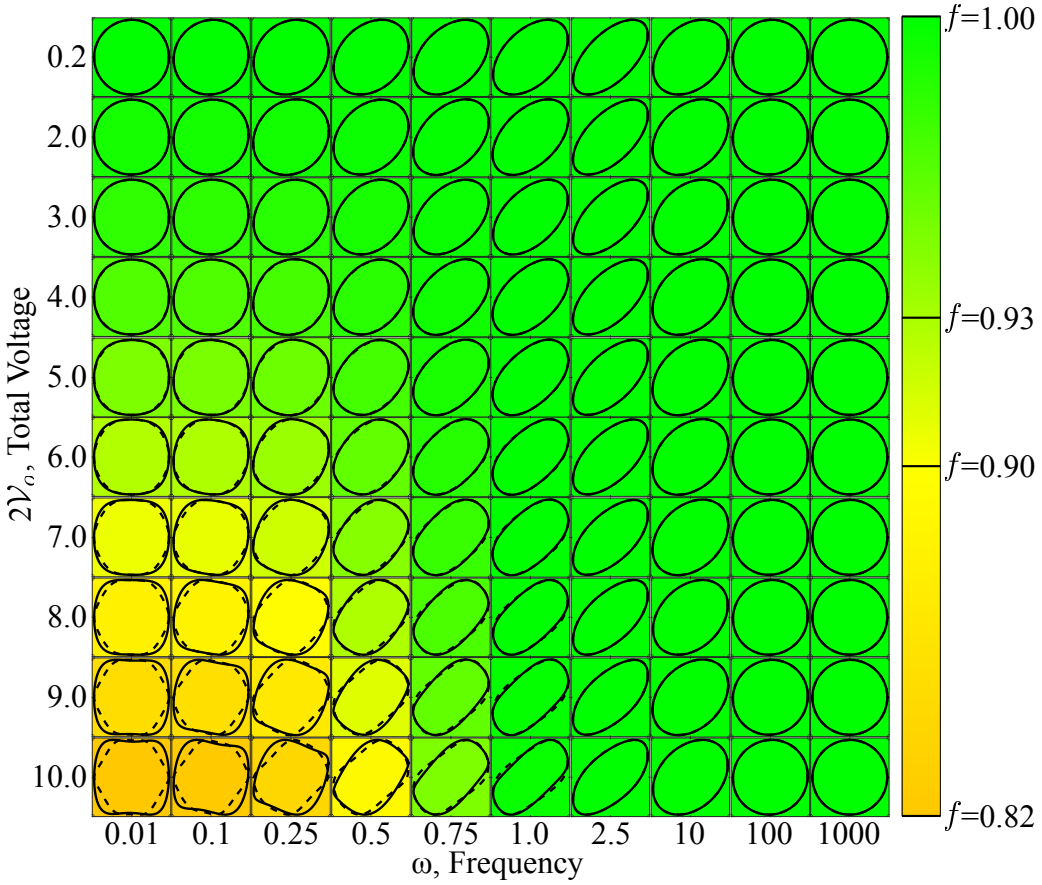

FIG. 5: (Color online) Pipkin diagram for $\epsilon = 0.25$. The solid and dashed lines represent the moderately nonlinear calculations and the numerical solutions, respectively. The color legend is the same as in figure 4. Also labeled on the color bar is $f = 0.93$, which is the value corresponding to $2\mathcal{V}_o = 6$ and $\omega = 0.01$.

Given that the current is $I(t) = \mathcal{V}_o I^{(1)}(t) + \mathcal{V}_o^3 I^{(3)}(t)$, it is natural to assume a similar expression for $\mathcal{Z}$ is

$$\mathcal{Z} = \mathcal{Z}^{(0)} + \mathcal{V}_o^2 \mathcal{Z}^{(2)} + O(\mathcal{V}_o^4). \tag{25}$$

This expression provides an approximation to the voltage dependence observed in impedance measurements at large voltages[25–27]. We can express $\mathcal{Z}$ in terms of the components of the electrostatic potential,

$$\mathcal{Z} = \frac{1}{\mathrm{i}\omega}\left[\frac{1}{\mathrm{d}\phi_1^{(1)}/\mathrm{d}x} - \mathcal{V}_o^2 \frac{\mathrm{d}\phi_1^{(3)}/\mathrm{d}x}{(\mathrm{d}\phi_1^{(1)}/\mathrm{d}x)^2}\right]. \tag{26}$$

Figure 8 are plots of $\mathrm{Im}(\mathcal{Z})$ and $\mathrm{Re}(\mathcal{Z})$ versus ω for $\epsilon = 0.025$ and 0.25 and $\mathcal{V}_o = 0.1$ and 3. At high frequency, the imaginary impedances are equal due to the aforementioned capacitance of the dielectric dominating the response. For small frequencies, however, the impedances are unequal.

The low frequency impedance increases with increasing Debye layer thickness. The imaginary part increases due to a reduction in capacitance and the real part due to an increased resistance - both due to less ions in the electrolyte. The decrease in $\mathrm{Im}(\mathcal{Z})$ with increasing voltage for both values of ϵ is due to the behavior of the Debye layer as a nonlinear capacitor. As voltage increases, the capacitance also increases. Since $\mathrm{Im}(\mathcal{Z})$ is inversely proportional to capacitance, it decreases[27]. For $\epsilon = 0.25$, this decrease is less pronounced than for $\epsilon = 0.025$ because of the lower ion concentration in the thick Debye layer case.

From figure 8b, $\mathrm{Re}(\mathcal{Z})$ is shown to increase with increasing voltage, for both values of ϵ, which corresponds to an increase in resistance. This can be attributed directly to the neutral salt adsorption from the bulk solution into the Debye layers at $O(\mathcal{V}_o^2)$. This causes a reduction in conductivity and hence an increase in $\mathrm{Re}(\mathcal{Z})$. Since there are fewer ions in solution in the $\epsilon = 0.25$ case, any ions adsorbed into the Debye layers represent a greater proportion of the total ion concentration. Hence, the increase in resistance is greater for $\epsilon = 0.25$.

V. CONCLUSIONS

We have quantified diffuse charge dynamics of a symmetric binary electrolyte at moderately nonlinear AC

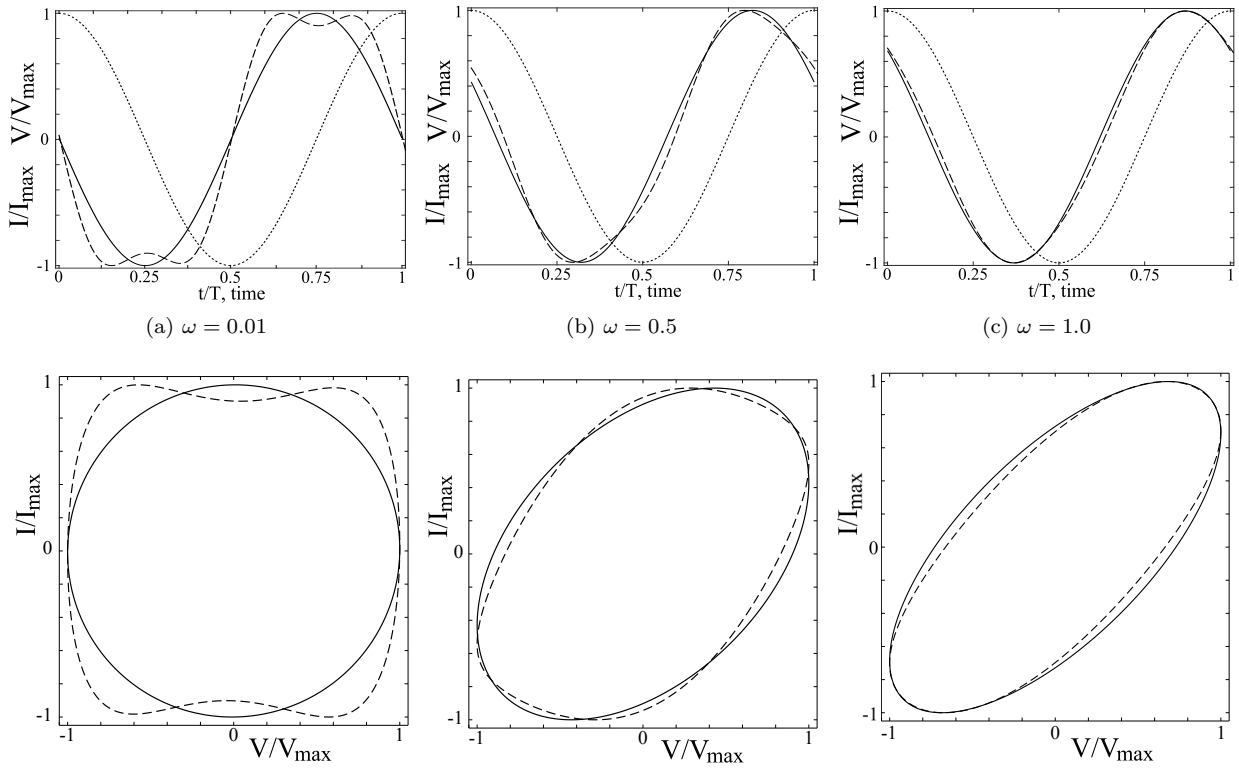

(a) $\omega = 0.01$ (b) $\omega = 0.5$ (c) $\omega = 1.0$

(d) $\omega = 0.01$ (e) $\omega = 0.5$ (f) $\omega = 1.0$

FIG. 6: Dependence of current on frequency. Solid lines are linear dynamics ($\mathcal{V}_o = 0.1$), dashed lines are moderately nonlinear ($\mathcal{V}_o = 3$), and dotted lines are the applied voltage. The "double-peak" visible in (a) and the "bow-tie" in (d) are due to the third harmonic of current. This harmonic gradually loses amplitude relative to the linear contribution as frequency increases.

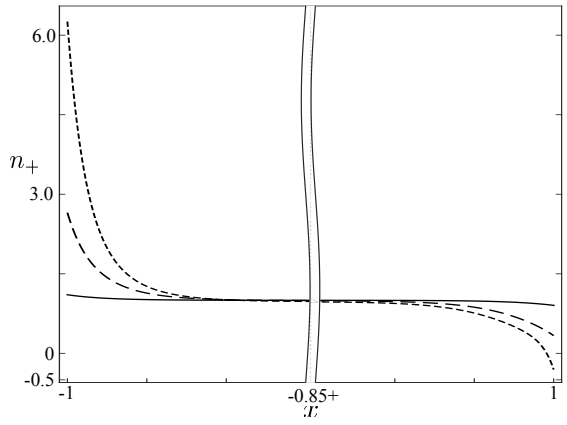

FIG. 7: Total cation density for $\omega = 0.01$ and $t = 0$ at three voltages: $\mathcal{V}_o = 0.1$ (solid), $\mathcal{V}_o = 1$ (dashed), and $\mathcal{V}_o = 2$ (dotted). As the voltage increases, the ion density becomes less antisymmetric and for $\mathcal{V}_o = 2$ attains a negative value at $x = 1$.

voltages. We used a Fourier series expansion in driving frequency for which the coefficients are expressed as a perturbation series in voltage amplitude. This approach allows the evaluation of nonlinearities in terms of both voltage order and harmonic mode. We find that the odd voltage orders have antisymmetric ion densities and electrostatic potential profiles. For symmetric electrolytes, the even voltage orders have ion densities that are symmetric and equal while the electrostatic potential is zero.

The symmetry in the $O(\mathcal{V}_o^2)$ ion densities represents "AC capacitive desalination"[27] in which neutral salt from the bulk solution adsorbs into the diffuse charge layers near the electrodes. The result is a reduced total salt concentration in the bulk and an increased resistance. Moreover, the net, or time averaged, separation of neutral salt is captured by the steady $O(\mathcal{V}_o^2)$ contribution.

We use our expansion to express a voltage dependent impedance. For low frequencies, we observe the increased bulk resistance manifesting as an increase in the real part of the impedance. The imaginary part of the impedance decreases with voltage due to the increase in Debye layer capacitance as predicted by Gouy-Chapman theory.

In this work, we considered a binary symmetric electrolyte, for simplicity. Asymmetry could be introduced through unequal ion valences or diffusivities, which would

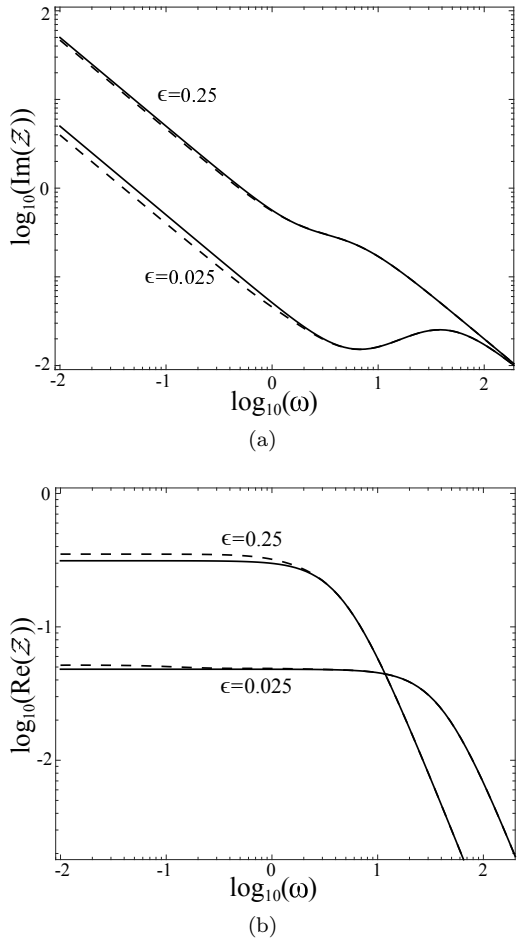

FIG. 8: Imaginary (a) and real (b) parts of the generalized impedance defined in (24) versus frequency of applied voltage for $\epsilon = 0.025$ and 0.25. The voltages plotted are $\mathcal{V}_o = 0.1$ (solid) and $\mathcal{V}_o = 3$ (dashed).

require only minor modification to our moderately nonlinear expansions. Such asymmetry would result in a non-zero $O(\mathcal{V}_o^2)$ potential, and hence unequal neutral salt adsorption and an $O(\mathcal{V}_o^2)$ contribution to the current. In addition, it would be interesting to consider modified PNP equations that account for ion-size effects [33] and ion-ion electrostatic correlations [34]. In the former case, various modified PNP equations including finite-ion-size effects predict a Debye layer capacitance that only weakly increases with voltage, in contrast to the exponential increase of the capacitance from Gouy-Chapman theory. Clearly, ion steric effects would thus dramatically impact the low-frequency impedance at large voltages. Finally, future work could also incorporate asymmetrically applied voltages and non-zero native zeta potentials to model asymmetric electrochemical supercapacitors, where the electrodes are made of differing materials.

ACKNOWLEDGEMENTS

Acknowledgment is made to the Donors of the American Chemical Society Petroleum Research Fund for partial support of this research. We also acknowledge NSF CAREER support under CBET-1350647.

[1] P. M. Biesheuvel and M. Z. Bazant, Phys. Rev. E. **81**, 031502 (2010).
[2] A. Mani and M. Z. Bazant, Phys. Rev. E **84**, 061504 (2011).
[3] Y. Oren, Desalination. **228**, 10 (2008).
[4] M. E. Suss, T. F. Baumann, W. L. Bourcier, C. M. Spadaccini, K. A. Rose, J. G. Santiago, and M. Stadermann, Energy Environ. Sci., **5**, 9511 (2012).
[5] T. M. Squires and S. R. Quake, Rev. Mod. Phys. **77**, (2005).
[6] J. A. Levitan, S. Devasenathipathy, V. Studer, Y. Ben, T. Thorsen, T. M. Squires, and M. Z. Bazant, Colloids Surf. A **267**, 122 (2005).
[7] A. Ramos, H. Morgan, N. G. Green, A. Gonzalez, and A. Castellanos, J. Appl. Phys. **97**, 084906 (2005).
[8] T. M. Squires and M. Z. Bazant, J. Fluid Mech. **509**, 217 (2004).
[9] M. Z. Bazant and T. M. Squires, Phys. Rev. Lett. **92**, 066101 (2004).
[10] T. M. Squires and M. Z. Bazant, J. Fluid Mech. **560**, 65 (2006).
[11] M. Mittal, P. P. Lele, E. W. Kaler, and E. M. Furst, J. Chem. Phys. **129**, 064513 (2008).
[12] D. C. Prieve, P. J. Sides, and C. L. Wirth, Curr. Opin. Colloid Interface Sci. **15**, 160 (2010).
[13] P. K. Wong, T. H. Wang, J. H. Deval, and C. M. Ho, IEEE/ASME Trans. Mechatron. **9**, 366 (2004).
[14] J. Voldman, Annu. Rev. Biomed. Eng. **8**, 425 (2006).
[15] M. Z. Bazant, K. Thornton, and A. Ajdari, Phys. Rev. E, **70**, 021506 (2004).
[16] J. Lyklem, *Fundamentals of Interface and Colloid Science. Volume II: Solid-Liquid Interfaces* (Academic Press, 1995).
[17] A. Ajdari, Phys. Rev. E **61**, R45 (2000).
[18] M. Z. Bazant, M. S. Kilic, B. D. Storey, and A. Ajdari, Adv. Colloid Interfac. **152**, 48 (2009).
[19] N. A. Mishchuk, T. Heldal, T. Volden, J. Auerswald, and H. Knapp, Microfluid. Nanofluid. **11**, 675 (2011).
[20] C. C. Huang, M. Z. Bazant, and T. Thorsen, Lab Chip **10**, 80 (2010).
[21] J. S. Paustian, A. J. Pascall, N. M. Wilson, and T. M. Squires, Lab Chip **14**, 3300 (2014).
[22] H. D. Abruña, Y. Kiya, and J. C. Henderson, Phys. Today **61**, 43 (2008).
[23] R. Kötz and M. Carlen, Electrochim. Acta **45**, 2483 (2000).
[24] A. Lasia, *Electrochemical Impedance Spectroscopy and its Applications*, (Springer, New York, NY, 2014).
[25] B. A. Yezer, A. S. Khair, P. J. Sides, and D. C. Prieve, J. Colloid Interface Sci. **449**, 2 (2015).
[26] F. C. M. Freire, G. Barbero, and M. Scalerandi, Phys. Rev. E, **73**, 051202 (2006).

[27] L. H. Olesen, M. Z. Bazant, and H. Bruus, Phys. Rev. E, **82**, 011501 (2010).
[28] O. Schnitzer and E. Yariv, Phys. Rev. E, **89**, 032302 (2014).
[29] L. Fan. Y. Liu, J. Xiong, H. S. White, and S. Chen, ACS Nano **8**, 10426 (2014).
[30] A. Bandopadhyay, V. A. Shaik, and S. Chakraborty, Phys. Rev. E, **91**, 042307, (2015).
[31] W. B. Russel, D. A. Saville, and W. R. Schowalter, *Colloidal Dispersions.* Cambridge University Press (1989).
[32] R. H. Ewoldt, A. E. Hosoi, and G. H. McKinley, J. Rheol. **52**, 1427 (2008).
[33] M. S. Kilic, M. Z. Bazant, and A. Ajdari, Phys. Rev. E. **75**, 021502 (2007).
[34] M. Z. Bazant, B. D. Storey, and A. A. Kornyshev, Phys. Rev. Lett. **106**, 046102 (2011).